

# Stimulated emission from multilayer graphene

Ken-ichi Sasaki\*

*NTT Research Center for Theoretical Quantum  
Physics and NTT Basic Research Laboratories,  
NTT Corporation, 3-1 Morinosato Wakamiya,  
Atsugi, Kanagawa 243-0198, Japan*

Kenichi Hitachi

*NTT Basic Research Laboratories, NTT Corporation,  
3-1 Morinosato Wakamiya, Atsugi, Kanagawa 243-0198, Japan*

Masahiro Kamada

*Advanced Research Laboratory, Anritsu Corporation,  
5-1-1 Onna, Atsugi, Kanagawa 243-8555, Japan*

Takamoto Yokosawa

*Advanced Research Laboratory, Anritsu Corporation,  
5-1-1 Onna, Atsugi, Kanagawa 243-8555, Japan*

Taisuke Ochi

*Advanced Research Laboratory, Anritsu Corporation,  
5-1-1 Onna, Atsugi, Kanagawa 243-8555, Japan*

Tomohiro Matsui†

*Advanced Research Laboratory, Anritsu Corporation,  
5-1-1 Onna, Atsugi, Kanagawa 243-8555, Japan*

(Dated: November 23, 2022)

## Abstract

Monolayer graphene absorbs 2.3 percent of the incident visible light. This “small” absorption has been used to emphasize the visual transparency of graphene, but it in fact means that multilayer graphene absorbs a sizable fraction of incident light, which causes non-negligible fluorescence. In this paper, we formulate the light emission properties of multilayer graphene composed of tens to hundreds of layers using a transfer matrix method and confirm the method’s validity experimentally. We could quantitatively explain the measured contrasts of multilayer graphene on  $\text{SiO}_2/\text{Si}$  substrates and found sizable corrections, which cannot be classified as incoherent light emissions, to the reflectance of visible light. The new component originates from stimulated emission caused by absorption at each graphene layer. Multilayer graphene thus functions as a partial coherent light source of various wavelengths, and it may have surface-emitting laser applications.

## I. INTRODUCTION

Visual detection of graphene on Si substrates is a common task, but it has the aspect of being a nontrivial scientific problem related to the interference effects of light.<sup>1-3</sup> The difference between the reflectance from the substrate and from the graphene on it has to be large enough to increase their contrast, and it is known that Si substrates with a certain thickness of SiO<sub>2</sub> ( $d_{\text{SiO}_2}$ ) have some advantage in this regard.<sup>4,5</sup> Namely, when the optical distance of the SiO<sub>2</sub> layer is one-half (or three-halves) the light wavelength used, not only are the two reflectances minimized by destructive interference but their difference (contrast) reaches a maximum. The physics behind this increase in the visibility of graphene is useful not just for searching for graphene but also for exploring notable phenomena. Namely, for example, we show that the reflectance of 20 layers of graphene on SiO<sub>2</sub>/Si substrate can become zero for normally incident visible light with a wavelength  $\lambda \simeq 2d_{\text{SiO}_2}$ . Zero reflectance is achieved with the destructive interference caused by SiO<sub>2</sub> and additional interference from multilayer graphene.<sup>5</sup> Usually, the interference of light is significant when there is a path difference on the order of a wavelength, but it may be sizable even when the path difference is much shorter than a wavelength (the thickness of 20-layer graphene is only  $\sim 6$  nm). Such a peculiar situation can be realized in a system with a large absorption coefficient, like graphene.<sup>6-8</sup> More importantly, the reflectance of such a system is determined complexly because a large absorption may produce non-negligible luminescence which also works as a secondary light source leading to more sophisticated interference effects of light.<sup>9-14</sup>

In this paper, we use a transfer-matrix method to define coherent and incoherent corrections to the reflectance of multilayer graphene on SiO<sub>2</sub>/Si substrates that are caused by light emission after the graphene absorbs the incident light. By comparing the calculated and measured contrasts (reflectivities) for various layer numbers, we identify the dependence of the coherent and incoherent components on the number of layers ( $N$ ). We find that even though the branching ratio of the coherent light emission to the absorbed energy is less than one percent, the coherent components become a main part of the corrections to the reflectance due to the nature of its coherence that enhances the reflection amplitude by additive interference. The origin of the coherent components is coherent photon emission stimulated by the incident light, while the incoherent ones are loosely related to Raman scattering.

Multilayer graphene composed of tens to hundreds of layers is an interesting research subject. However, it has not been explored much, partly because the success of the exfoliation method has rapidly shifted the interest of many researchers from infinite layers of graphite to few-layer graphene. The obvious advantage of multilayer graphene is that it can increase signal strength, whereas the signal strength of few-layer graphene is low and difficult to measure. Besides that, there are intriguing phenomena. For example, it has been shown that the number of layers that best absorb infrared radiation is 87.<sup>15</sup> It is also very interesting that a large nonlinear optical effect is being discussed as an effect peculiar to multilayer graphene.<sup>16–18</sup> For example, Yang *et al.* demonstrated that 24 layers of graphene on a quartz substrate yields the maximum third-harmonic signal.<sup>19</sup>

This paper is organized as follows. In Sec. II, we review the reflectance without light emission, which provides a starting point of this study. The theory includes only the light scattering and absorption caused by dynamical conductivity of each graphene layer and the substrate. We pay special attention to the result that the reflectance of 20 layers of graphene on SiO<sub>2</sub>/Si substrate can become zero for normally incident visible light with a wavelength  $\lambda \simeq 2d_{\text{SiO}_2}$ , because the system is most useful for exploring the corrections to the reflectance. In Sec. III, we examine the corrections to the reflectance due to light emissions. The contributions of light emissions to the reflectance are divided into two categories in terms of the coherence, where coherent emission corresponds to stimulated emission with a common phase, while incoherent emission with a random phase is identified as Raman scattering. The comparison between calculated and measured contrasts is shown in Sec. IV. Our discussion and conclusion are provided in Sec. V.

## II. REFLECTANCE WITHOUT LIGHT EMISSION

Because of the conical energy-band structure of graphene known as the Dirac cone, the dynamical conductivity is well approximated by  $\pi\alpha\epsilon_0c$  for visible light,<sup>20</sup> where  $\alpha$  is the fine-structure constant ( $\sim 1/137$ ). As a result, monolayer graphene absorbs  $\sim 2.3$  percent ( $= \pi\alpha$ ) of the incident visible light.<sup>21</sup> By a straightforward calculation of the Kubo formula, with the understanding that the effect of the stacking order on the reflectance appears in the infrared regime,<sup>22–24</sup> the dynamical conductivity of graphite is given by that of graphene divided by the interlayer spacing  $d$  (0.335 nm) as  $\sigma_{\text{graphite}} = \frac{\pi\alpha\epsilon_0c}{d}$ .<sup>15,25</sup> Thus, the relative

permittivity of graphite is given by

$$\varepsilon_g = \varepsilon_r + i \frac{\alpha \lambda}{2d}, \quad (1)$$

for visible light wavelengths  $\lambda$ , where  $\varepsilon_r$  is the dielectric constant of the interlayer space. If the interlayer space is a vacuum, an appropriate choice would be  $\varepsilon_r = 1$ . However, because the electronic wave function of the  $\pi$ -orbital spreads into the interlayer space, light propagating in it is subjected to the spread of the wave function. To compensate for this, we assume  $\varepsilon_r = 4$  [see Appendix A for details].<sup>26,27</sup> Although  $\alpha$  is certainly a small quantity, since visible light has a much longer  $\lambda$  (400~800 nm) than  $d$ , the imaginary part of  $\varepsilon_g$  is above the real part  $\varepsilon_r$ . This characterizes the optical properties of multilayer graphene.

For the system shown in Fig. 1(a), the reflectance to normally incident light of wavelength  $\lambda$  coming from air is formulated using the reflection coefficient  $c_N^r(\lambda)$  as  $R_N(\lambda) = |c_N^r(\lambda)|^2$ , where

$$c_N^r(\lambda) = \frac{\left[ (1 - n_{\text{Si}}) \cos \varphi - i \left( \frac{n_{\text{Si}}}{n_{\text{SiO}_2}} - n_{\text{SiO}_2} \right) \sin \varphi \right] \cos \phi - \left[ \left( \frac{n_{\text{SiO}_2}}{\sqrt{\varepsilon_g}} - \frac{n_{\text{Si}} \sqrt{\varepsilon_g}}{n_{\text{SiO}_2}} \right) \sin \varphi + i \left( \frac{n_{\text{Si}}}{\sqrt{\varepsilon_g}} - \sqrt{\varepsilon_g} \right) \cos \varphi \right] \sin \phi}{\left[ (1 + n_{\text{Si}}) \cos \varphi - i \left( \frac{n_{\text{Si}}}{n_{\text{SiO}_2}} + n_{\text{SiO}_2} \right) \sin \varphi \right] \cos \phi - \left[ \left( \frac{n_{\text{SiO}_2}}{\sqrt{\varepsilon_g}} + \frac{n_{\text{Si}} \sqrt{\varepsilon_g}}{n_{\text{SiO}_2}} \right) \sin \varphi + i \left( \frac{n_{\text{Si}}}{\sqrt{\varepsilon_g}} + \sqrt{\varepsilon_g} \right) \cos \varphi \right] \sin \phi}. \quad (2)$$

Here,  $\varphi \equiv n_{\text{SiO}_2} d_{\text{SiO}_2} \frac{2\pi}{\lambda}$  is the phase acquired by light after it propagates through a distance  $d_{\text{SiO}_2}$  in  $\text{SiO}_2$ , and  $\phi \equiv \sqrt{\varepsilon_g} \frac{2\pi}{\lambda} d_N$  is the complex phase acquired when light passes through  $N$ -layer graphene of thickness  $d_N = Nd$ .<sup>28</sup>  $n_{\text{Si}}$  and  $n_{\text{SiO}_2}$  are the refractive indexes of Si and  $\text{SiO}_2$ , respectively. Si is treated as an absorbing substrate ( $n_{\text{Si}}$  is a complex number) whose dispersion is taken into account,<sup>29</sup> while  $\text{SiO}_2$  is treated as an absorption-free film with dispersion.<sup>30</sup> The  $R_N(\lambda)$  value depends sensitively on the two phases,  $\varphi$  and  $\phi$ . When  $N = 0$  or  $\phi = 0$  in Eq. (2),  $R_0(\lambda)$  corresponds to the reflectance of the substrate without graphene. It can be minimized for specific  $\lambda$  by destructive interference; namely,  $R_0(\lambda)$  is at a minimum when  $\cos \varphi = 0$  as  $\left| \frac{n_{\text{Si}} - n_{\text{SiO}_2}^2}{n_{\text{Si}} + n_{\text{SiO}_2}^2} \right|^2$ .<sup>28</sup> Monolayer graphene is most easily detectable on  $\text{SiO}_2/\text{Si}$  substrates when destructive interference occurs, because  $|R_0(\lambda) - R_1(\lambda)|$  takes a maximum when  $\cos \varphi = 0$ .<sup>4</sup>

The complex phase  $\phi$  causes a further suppression of the reflectance beyond that of  $\varphi$ . Intriguingly, when destructive interference takes place ( $\varphi = 3\pi/2$ ),  $R_N(\lambda)$  vanishes for  $N \simeq 20$  and  $\lambda \simeq 2d_{\text{SiO}_2}$  [see Fig. 1(b)], which has been referred to as zero reflection.<sup>5,28</sup>

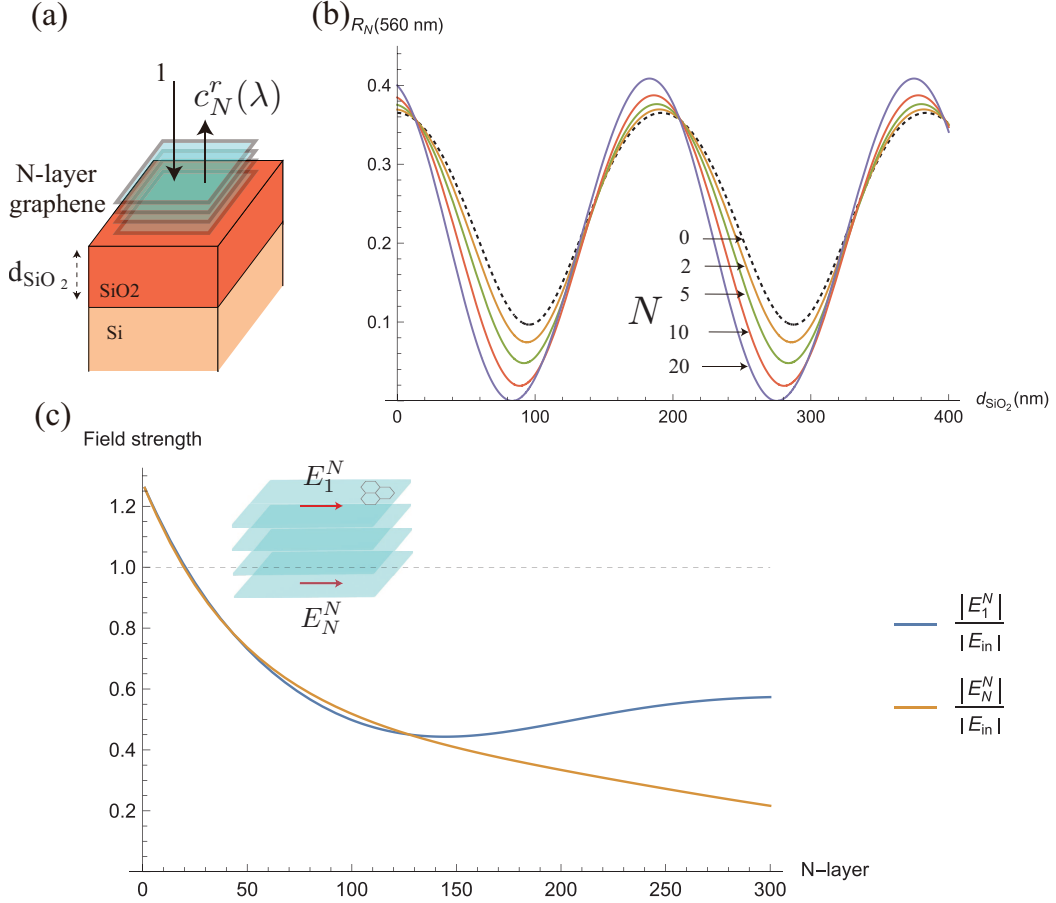


FIG. 1. **Basic optical properties of  $N$ -layer graphene on  $\text{SiO}_2/\text{Si}$  substrate.** (a) Schematic diagram of  $N$ -layer graphene on top of the substrate, where the Si layer has a semi-infinite thickness. The case of  $N = 0$  means the reflectance of the substrate without graphene. (b)  $R_N(560 \text{ nm})$  as a function of  $d_{\text{SiO}_2}$  for different values of  $N$ . Light of  $\lambda = 560 \text{ nm}$  is not reflected when  $N = 20$  at  $d_{\text{SiO}_2} \sim 275 \text{ nm}$ . (c) The electric field strength of the top and bottom layers of  $N$ -layer graphene on substrate with  $d_{\text{SiO}_2} = 275 \text{ nm}$ .

Even though 20-layer graphene on the substrate does not reflect light of  $\lambda \simeq 2d_{\text{SiO}_2}$ , it is detectable because of a large contrast. To capture the essential role of graphene in achieving zero reflection, let us first consider Eq. (2) when  $\cos \phi = 0$ . For the numerator to vanish,  $i(n_{\text{Si}} - n_{\text{SiO}_2}^2) \cos \phi - \left( \frac{n_{\text{SiO}_2}^2}{\sqrt{\epsilon_g}} - n_{\text{Si}} \sqrt{\epsilon_g} \right) \sin \phi = 0$  has to be satisfied. Since  $\phi$  is small, this equation can be simplified as  $i(n_{\text{Si}} - n_{\text{SiO}_2}^2) - (n_{\text{SiO}_2}^2 - n_{\text{Si}} \epsilon_g) \frac{d}{\lambda} 2\pi N = 0$ , which shows that  $N \sim \frac{1}{\pi \alpha} \left( 1 - \frac{n_{\text{SiO}_2}^2}{n_{\text{Si}}} \right)$  is an approximate layer number that gives zero reflection. This argument makes it easy to understand that the dominant imaginary part of  $\epsilon_g$  ( $\simeq i\alpha\lambda/2d$ ) is essential

to the existence of zero reflection. Second, we plot the electric field strength of the top and bottom layers of  $N$ -layer graphene on the substrate in Fig. 1(c). The crossing point with the dashed line,  $|E_j^N|/|E_{\text{in}}| = 1$ , where  $E_{\text{in}}$  denotes the electric field of the incident light, shows the special zero-reflection feature that the induced field component is completely absorbed by 20-layer graphene.

### III. CORRECTIONS TO REFLECTANCE BY LIGHT EMISSION

The corrections to the reflectance are the main subjects of this paper.<sup>9,10</sup> Specifically, we consider the corrections where some fraction of the energy absorbed by the  $j$ th layer is transferred to light emitted from that layer [see Fig. 2(a)]. The amplitude of emitted light is assumed to be the square root of the layer absorption,<sup>25</sup>  $A_j^N \equiv \pi\alpha|E_j^N|^2/|E_{\text{in}}|^2$ , multiplied by the branching ratio,  $\mathcal{B}$ , i.e.,  $\sqrt{(\mathcal{B}/2) A_j^N}$ , where  $1/\sqrt{2}$  means that light emission is direction-independent along the  $c$ -axis. Note that  $A_j^N$  depends not only on  $j$  and  $N$  values [Fig. 1(c)] but also on  $\lambda$  and  $d_{\text{SiO}_2}$ .<sup>15</sup>

To examine the effect of light emission from the  $j$ th layer on the reflectance, we define two subsystems, as shown in Fig. 2(b): one is an isolated  $(j - 1)$ -layer graphene in air; the other is  $(N - j)$ -layer graphene on the  $\text{SiO}_2/\text{Si}$  substrate. Using the transfer matrix method, we can obtain the transmission and reflection coefficients of an isolated  $(j - 1)$ -layer graphene in air [ $c_{j-1}^{tg}$  and  $c_{j-1}^{rg}$ ] and the reflection coefficient of  $(N - j)$ -layer graphene on the  $\text{SiO}_2/\text{Si}$  substrate [ $c_{N-j}^r$ ].<sup>15,25</sup> Let the reflection coefficients be  $X_j$  and  $Y_j$  and transmission coefficient be  $Z_j$  for the combined subsystems [see Fig. 2(b)]. These can be obtained by a self-consistent method as follows. After calculating  $X_j^{(n)}$ , we add it to  $\sqrt{(\mathcal{B}/2) A_j^N}$  of the incident light to the  $(j - 1)$ -layer graphene (in air) as  $\sqrt{(\mathcal{B}/2) A_j^N} + X_j^{(n)}$  and recalculate  $Y_j^{(n+1)} = c_{j-1}^{rg} \left( \sqrt{(\mathcal{B}/2) A_j^N} + X_j^{(n)} \right)$  and  $Z_j^{(n+1)} = c_{j-1}^{tg} \left( \sqrt{(\mathcal{B}/2) A_j^N} + X_j^{(n)} \right)$ . Then, we add a new  $Y_j^{(n+1)}$  to  $\sqrt{(\mathcal{B}/2) A_j^N}$  of the light incident to the  $(N - j)$ -layer graphene on the  $\text{SiO}_2/\text{Si}$  substrate as  $\sqrt{(\mathcal{B}/2) A_j^N} + Y_j^{(n+1)}$  and recalculate  $X_j^{(n+1)} = c_{N-j}^r \left( \sqrt{(\mathcal{B}/2) A_j^N} + Y_j^{(n+1)} \right)$ . These computations are repeated until  $X_j$  and  $Y_j$  converge. In this way, we can obtain an

analytical expression of the converged  $X_j$ ,  $Y_j$ , and  $Z_j$  for a given  $\mathcal{B}$  as

$$\begin{aligned}
X_j(\mathcal{B}) &= c_{N-j}^r \left\{ \frac{1 + c_{j-1}^{rg}}{1 - c_{N-j}^r c_{j-1}^{rg}} \right\} \sqrt{\left(\frac{\mathcal{B}}{2}\right) A_j^N}, \\
Y_j(\mathcal{B}) &= c_{j-1}^{rg} \left\{ \frac{1 + c_{N-j}^r}{1 - c_{N-j}^r c_{j-1}^{rg}} \right\} \sqrt{\left(\frac{\mathcal{B}}{2}\right) A_j^N}, \\
Z_j(\mathcal{B}) &= c_{j-1}^{tg} \left\{ \frac{1 + c_{N-j}^r}{1 - c_{N-j}^r c_{j-1}^{rg}} \right\} \sqrt{\left(\frac{\mathcal{B}}{2}\right) A_j^N}.
\end{aligned} \tag{3}$$

The (corrected) electric field at an infinitesimal distance above and below the  $j$ th layer becomes  $\sqrt{(\mathcal{B}/2) A_j^N} + X_j^{(n)} + Y_j^{(n+1)}$  and  $\sqrt{(\mathcal{B}/2) A_j^N} + Y_j^{(n)} + X_j^{(n+1)}$ , respectively. Self-consistency, such as  $\lim_{n \rightarrow \infty} X_j^{(n)} = X_j$  and  $\lim_{n \rightarrow \infty} Y_j^{(n)} = Y_j$ , is therefore essential to ensure that the (corrected) electric field is continuous at the  $j$ th layer, which is a requirement of the Maxwell equations.

$Z_j(\mathcal{B})$  is the value at the zero initial phase, so the transmission coefficient can be given a phase degree of freedom expressing the coherence or incoherence of photon emissions from the different layers:

$$z_N \equiv \sum_{j=1}^N e^{i\theta_j} Z_j(\mathcal{B}). \tag{4}$$

Accordingly, the corrected reflectance is uniquely determined by  $R_N \equiv |c_N^r + z_N|^2 = |c_N^r|^2 + 2\text{Re}[c_N^r z_N^*] + |z_N|^2$ . The  $z_N$  value depends on these phases  $\theta_j$ .<sup>31</sup> For stimulated emission, the phase is given by a coherent phase as

$$e^{i\theta_j} = -\frac{(E_j^N)^*}{|E_j^N|}. \tag{5}$$

The right-hand side is separated into two factors. First,  $(E_j^N)^*$  is a result of the fact that the electric field in quantum field theory is a Hermitian operator expressed as  $\hat{E}(z_j, t) = \hat{E}_j^N e^{-i\omega t} + (\hat{E}_j^N)^\dagger e^{+i\omega t}$ . The field operator is expanded by positive and negative frequency modes,  $e^{-i\omega t}$  and  $e^{+i\omega t}$ , and the positive (negative) frequency mode annihilates (creates) a photon. Stimulated emission is relevant to photon creation of the second term. Since we are using a transfer matrix method to calculate the electric field, we implicitly assume a classical field given by the expectation value of annihilation and creation operators with respect to a coherent state; namely,  $\langle \hat{E}_j^N \rangle = E_j^N$  and  $\langle (\hat{E}_j^N)^\dagger \rangle = (E_j^N)^*$  as  $\langle \hat{E}(z_j, t) \rangle = E_j^N e^{-i\omega t} + (E_j^N)^* e^{+i\omega t}$ . Thus, the emitted (created) photon has an amplitude proportional

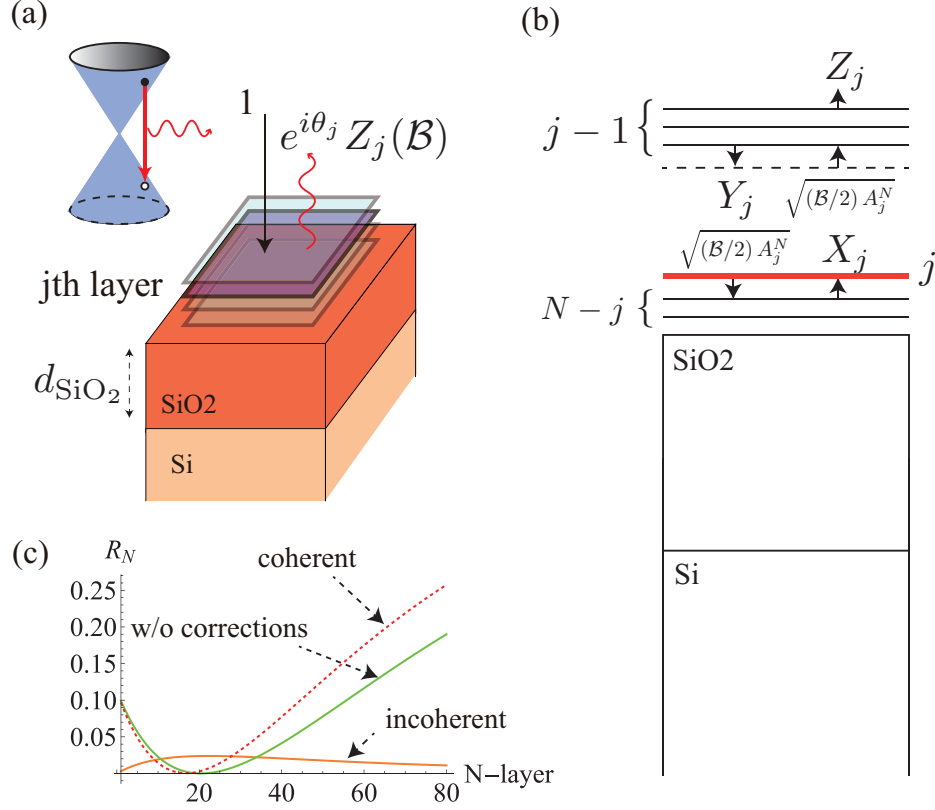


FIG. 2. **Light emission from  $N$ -layer graphene on  $\text{SiO}_2/\text{Si}$  substrate.** (a) Corrections to the reflectivity arise because some fraction of the electron-hole pairs created by the photon absorption emit light (luminescence). The corrections to the reflectivity of each layer are summed using Eq. (4). (b)  $Z_j$  is calculated self-consistently as explained in the text. (c) Dependence of the corrections to  $R_N(560 \text{ nm})$  [Eq. (8)] on  $N$ , where  $d_{\text{SiO}_2} = 275 \text{ nm}$ ,  $\mathcal{B}_{inc} = 0.1$ ,  $\mathcal{B}_{sti} = 0.0007$  and  $\theta = \pi$ . The incoherent components are enhanced (which is known as interference-enhanced Raman scattering) at around 20 layers.

to  $(E_j^N)^*$ . Second, the minus sign comes from the fact that the orientation of the dipole moment (or photocurrent) reverses for absorption and emission resonances.<sup>32,33</sup> For the direct interband transitions in the Dirac cone, the reversal is protected by particle-hole symmetry.<sup>34</sup> Actually, the phase lag between the driving field and dipole moment can take a general value depending on the scattering lifetime  $\tau$  of photoexcited carriers. For example, in analyzing graphite at telecom wavelengths, we do not expect  $-1$  to appear there, because interlayer interaction in graphite modifies the symmetry. We shall assign a phase parameter  $\theta$ , which is independent of  $j$ , to it. It is better not to fix the  $\theta$  value to  $\pi$  only, but here, we will

restrict ourselves to the case of  $\theta = \pi$ . Note that Eq. (5) is obtained with an assumption of the coherent state. Thus, Eq. (5) may be invalidated when, for example, the photon number is fixed and the phase becomes uncertain.

The reflectance corrected by stimulated emission leads to

$$R_N = \left| c_N^r + e^{i\pi} \sum_{j=1}^N \frac{(E_j^N)^*}{|E_j^N|} Z_j(\mathcal{B}_{sti}) \right|^2, \quad (6)$$

where  $\mathcal{B}_{sti}$  is the branching ratio of stimulated photon emission to absorbed photons. Since coherent photon emission is given by the annihilation of photo-excited electron-hole pairs by the electron-photon coupling strength,  $\mathcal{B}_{sti}$  should be insensitive to changes in  $N$ . Moreover, as shown in Fig. 2(c), the coherent corrections can make positive ( $N > 20$ ) and negative ( $N < 20$ ) contributions to the reflectance. This is because  $c_N^r$  changes its sign from + to - at  $N = 20$  of the zero reflection, while  $z_N$  is a negative (almost real) number (due to the  $\pi$  phase). Note that the coherent corrections slightly shift the layer number of zero reflection from 20, but that does not spoil the existence of zero reflection.

Next we apply  $R_N = |c_N^r|^2 + 2\text{Re}[c_N^r z_N^*] + |z_N|^2$  to the case that  $\theta_j$  in  $z_N$  is a random variable. The exact definition of random is that if we take the time average regarding  $\theta_j$ , we have  $\langle \text{Re}[c_N^r z_N^*] \rangle = 0$  and  $\langle |z_N|^2 \rangle = \sum_{j=1}^N |Z_j(\mathcal{B})|^2$ . We refer to this case as incoherent corrections. Indeed, from Eq. (4) we get an interference term in  $|z_N|^2$  as the last term of

$$|z_N|^2 = \sum_{i=1}^N |Z_i(\mathcal{B})|^2 + \sum_{i \neq j} e^{i(\theta_i - \theta_j)} Z_i(\mathcal{B}) Z_j^*(\mathcal{B}), \quad (7)$$

though it vanishes by taking the time average, and only the first term of the incoherent corrections will remain.<sup>35</sup> Commonly, inelastic scattering of light such as (spontaneous) Raman scattering is considered as incoherent photons. Namely, the reflectance of a specific light frequency ( $\omega$ ) undergoes the incoherent corrections especially when a white-light beam is used as an excitation source, since it contains various frequencies  $\omega_e$  above  $\omega$ , where  $\omega_e - \omega$  corresponds to the frequency of the Raman active phonon modes.<sup>36</sup> Let  $\mathcal{B}_{inc}$  be the branching ratio of incoherent photon emissions, in which light emitted from each layer contributes independently to the reflectance. Since  $Z_j(\mathcal{B}_{inc})$  is proportional to  $\sqrt{\mathcal{B}_{inc} A_j^N}$  [Eq. (3)], the incoherent corrections are proportional to  $\mathcal{B}_{inc} A_j^N$ . For Raman scattering, parameter  $\mathcal{B}_{inc}$  is fundamentally determined by the electron-photon and electron-phonon coupling strengths, and it should not be so sensitive to the change in  $N$ . Indeed, the incoherent corrections with

a constant  $\mathcal{B}_{inc}$  follow roughly the measured  $N$ -dependence of the G-band Raman intensity [Appendix C].

A generalized reflection formula covering the above two cases is written as

$$R_N(\lambda, \theta, \mathcal{B}_{sti}, \mathcal{B}_{inc}) \equiv \left| c_N^r + e^{i\theta} \sum_{j=1}^N \frac{(E_j^N)^*}{|E_j^N|} Z_j(\mathcal{B}_{sti}) \right|^2 + \sum_{j=1}^N |Z_j(\mathcal{B}_{inc})|^2. \quad (8)$$

When  $\mathcal{B}_{sti} = \mathcal{B}_{inc} = 0$ ,  $R_N(\lambda, \theta, \mathcal{B}_{sti}, \mathcal{B}_{inc})$  reduces to Eq. (2) with Eq. (1). Note that the incoherent corrections always increase the reflectance and preclude zero reflections [Fig. 2(c)], which is in contrast to the coherent corrections. Moreover, the G-band Raman intensity is enhanced when zero reflection occurs.<sup>10,37–39</sup> This is known as interference-enhanced Raman scattering,<sup>9</sup> which is reasonably reproduced by Eq. (8).

#### IV. COMPARISON BETWEEN CALCULATED AND MEASURED CONTRAST

Multilayer graphene was prepared by exfoliating highly oriented pyrolytic graphite (HOPG) on SiO<sub>2</sub>/Si substrate, and the thickness of the graphene flakes was determined by atomic force microscopy (Dimension XR, Bruker). The reflectance of the multilayer graphene was measured with a spectroscopic reflectometer (TohoSpec3100, Toho Technology) using an objective lens of  $\times 50$ . First, we determined that  $d_{\text{SiO}_2} = 268$  nm from the reflectance of the substrate (Appendix B). This value is used consistently in all the calculations reported in this paper.

We calculated Eqs. (2) and (8) for  $N$ -layer graphene with  $N = 0, 1, 4, 7, 14, 15, 18, 24, 26, 28, 37, 38, 40, 47, 54, 55, 60, 64, 65, 66, 70, 97, 108, 110, 122, 135, 160, 226, \text{ and } 319$  on the same SiO<sub>2</sub>/Si substrate. We compared the calculated results with measured contrasts ( $C_N \equiv R_N/R_0$ ) rather than reflectivities ( $R_N$ ) to avoid any artificial shift introduced for reflectivities (Appendix B). Representative measured spectral contrasts are presented by black dots in Fig. 3. The calculated contrasts are shown by the red curves, which include coherent corrections only. The green curves are for Eq. (2), which does not include any corrections. All calculations were performed with  $\mathcal{B}_{sti} = 0.0007$  [see Fig. 2(c)], where this value was chosen so that we could obtain good agreement between the calculations and observations for all layers. In particular, almost perfect agreements are seen for 7, 70, 122, 160, and 226 layers (and more).

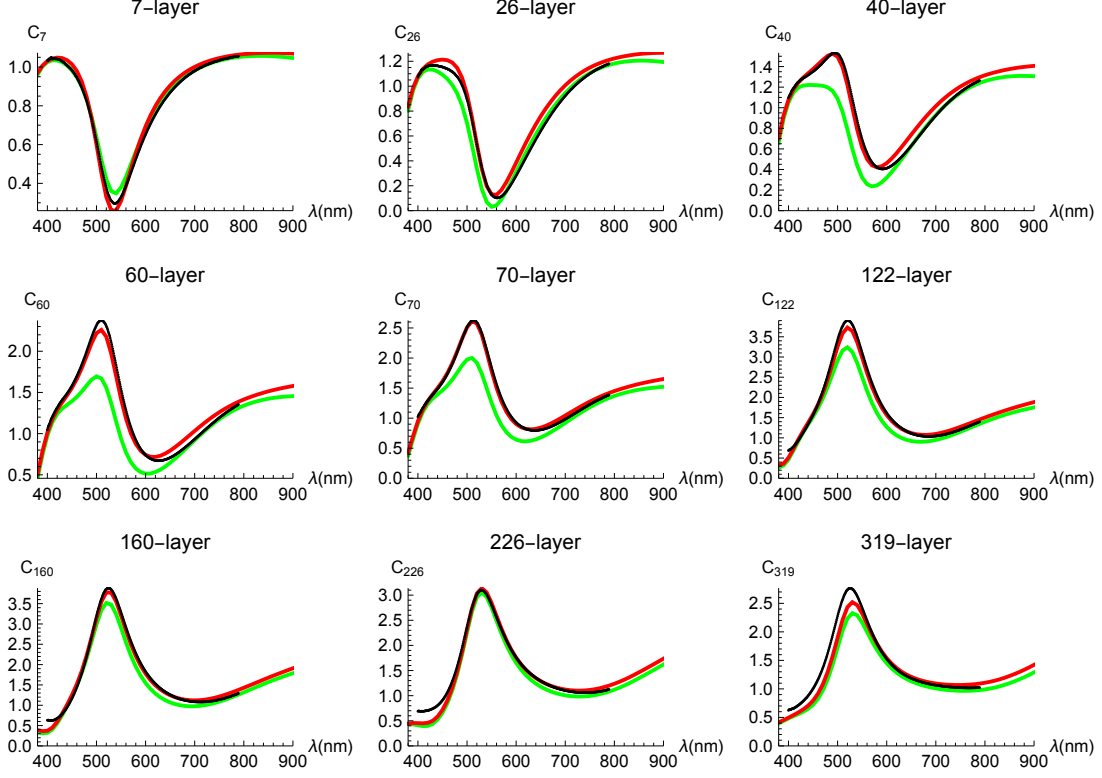


FIG. 3. Measured (black) and calculated (green and red) spectral contrasts of  $N$ -layer graphene on the same  $\text{SiO}_2/\text{Si}$  substrate. A white-light source was used, and the reflectivity was measured at room temperature. The green curves are for Eq. (2) which does not include corrections. The red curves include only coherent corrections. The horizontal axis is  $\lambda$  (nm), and the reliable range of our spectrometer is 450 to 800 nm.

From the good agreement between the calculated and measured contrasts shown in Fig. 3, we can draw two main conclusions. First, the  $\pi$ -phase ( $\theta = \pi$ ) of the coherent corrections is very essential. If we adopt 0-phase ( $\theta = 0$ ), serious discrepancy arises, which can be readily imagined from the relative location of the red curves with respect to the green ones. Strictly speaking, we can notice a slight deviation of the red curves from the black curves for 26 and 319 layers. In the case of 26 layers, a difference between the two curves appears only for  $\lambda > 560$  nm. In the case of 319 layers, a noticeable disagreement is seen only for  $\lambda < 540$  nm. It can be shown that a slight shift of  $\theta$  from  $\pi$  improves the fitting. This suggests a possibility that  $\theta$  has a small fluctuation around  $\pi$  depending on  $N$  and  $\lambda$ . Second, the incoherent corrections are basically small. In fact, for most layers examined (not shown in

Fig. 3), the incoherent corrections are unfavorable for improving the fitting. Our estimation of the reasonable range of  $\mathcal{B}_{inc}$  is less than 0.01. However, there are exceptions: for only 1, 4, and 24 layers (listed in the upper panels of Fig. 4), inclusion of incoherent corrections with  $\mathcal{B}_{inc} = 0.1$  improved the fitting as shown in the lower panels of Fig. 4, where the orange dashed curves include only incoherent corrections.

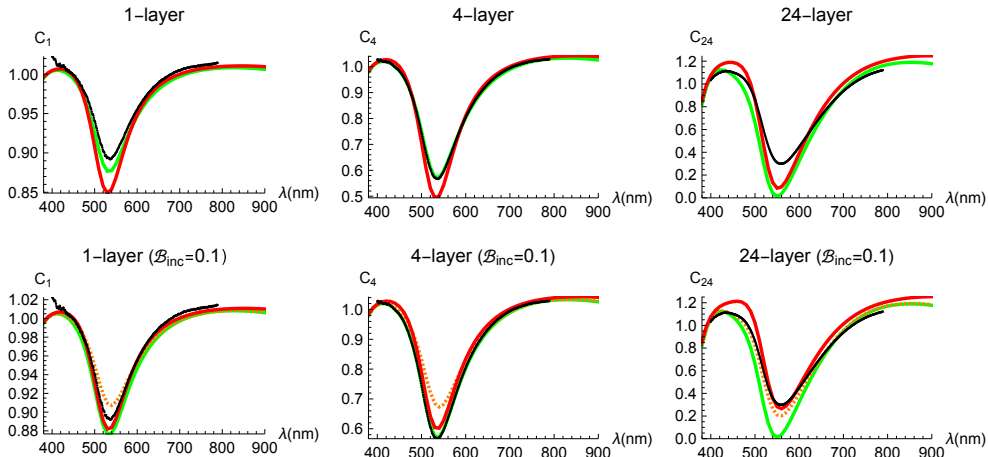


FIG. 4. **Exceptional case.** For only 1-, 4-, and 24-layer samples, neglecting the incoherent corrections (upper) does not give a reasonable agreement between the calculated and measured contrast. The incoherent corrections with  $\mathcal{B}_{inc} = 0.1$  (lower) improve the fitting. (lower) The orange dashed curves include only incoherent corrections. The red curves include both coherent and incoherent corrections.

In the lower panels of Fig. 4, when  $N$  is small (i.e. 1- and 4-layer samples), the large difference between green solid curve and orange dashed curve around the minimum shows that we are assuming sizable incoherent corrections. For the case of 4 layers in particular, this is apparently inconsistent with the measurement, as the orange dashed curve has a larger deviation from the black dots than the green curve does [Eq. (2) without corrections]. However, the incoherent corrections are partly canceled by the coherent ones. On the other hand, the green curve still has better agreement with the measured contrast. For the 24-layer sample, which is close to the invisible 20-layer graphene, the incoherent corrections can be significant. This is expected as the interference-enhanced Raman scattering. Meanwhile, it is not convincing to state that the coherent component improves the fitting. Naturally, it is hard to believe that  $\mathcal{B}_{inc}$  is enhanced only for these specific layer numbers. The discrepancy

between the measured and calculated values in the upper panels of Fig. 4 might suggest a small coverage of the graphene samples compared to the light spot size. Because  $R_N/R_0 < 1$  ( $N = 1, 4, 24$ ) around the minimum, the measured contrast tends to be overestimated as  $C_N \rightarrow [(1-x)R_N + xR_0]/R_0$  when  $x \neq 0$ . In other words, the calculations assume a large coverage with  $x = 0$ . To elucidate the origin of the large discrepancy between theory and experiment of 1-, 4-, and 24-layer samples, it will be useful to eliminate the incoherent corrections as much as possible. Since the incoherent corrections originate from inelastic scatterings such as Raman scattering, they must be suppressed by inserting a filter in front of a white-light source.

Since the incoherent corrections decrease with increasing  $N$  [Fig. 2(c)] and the coherent corrections dominate the incoherent ones above  $N = 40$  even if  $\mathcal{B}_{inc}$  is as large as 0.1, we may neglect the incoherent corrections above  $N = 60$ . Indeed, for the graphene samples more than 60 layers thick, the incoherent corrections with  $\mathcal{B}_{inc} = 0.1$  to the reflectivity are suppressed and negligible, and the coherent corrections to the reflectance are essential for improving the fitting.

## V. DISCUSSION AND CONCLUSION

The  $\pi$ -phase for stimulated emission had a direct influence on the optical properties, and the magnitude of stimulated emission  $\mathcal{B}_{sti}$  was extracted from experiments. These become more transparent by considering thin multilayer graphene suspended in air. For clarity, let us consider monolayer graphene whose reflection and transmission coefficients are  $c_1^r = -\pi\alpha/(2+\pi\alpha)$  and  $c_1^t = 2/(2+\pi\alpha)$ , and the absorption is given by  $A_1^1 = 1 - |c_1^r|^2 - |c_1^t|^2 = \pi\alpha/(1 + \pi\alpha/2)^2$ . The reflection coefficient is modified by stimulated emission as

$$c_1^r + e^{i\theta} Z_1(\mathcal{B}_{sti}) = -\frac{\frac{\pi\alpha}{2}}{1 + \frac{\pi\alpha}{2}} + e^{i\theta} \sqrt{\frac{\mathcal{B}_{sti}}{2} \frac{\pi\alpha}{(1 + \frac{\pi\alpha}{2})^2}}. \quad (9)$$

When  $\mathcal{B}_{sti} = 0.0007$ , the magnitude of the second term is 0.0028, which is about 25 percent of the magnitude of the first term (0.011). When  $\theta = \pi$ , the correction term is negative in sign, and therefore the reflectance is increased by stimulated emission. This contrasts with thin multilayer graphene on the  $\text{SiO}_2/\text{Si}$  substrate, which shows slightly suppressed reflectance. Interestingly, the destructive interference makes  $c_N^r$  a positive number for small  $N$  so that the reflectance is suppressed by stimulated emission. To observe the stimulated emission

as a correction to the reflectance, it is important that  $|c_N^r|$  be a small quantity, which is again provided by destructive interference in this paper. When constructive interference is realized,  $c_N^r$  is a negative number for small  $N$ , and stimulated emission would decrease the reflectance. However,  $|c_N^r|$  is not small then, so the corrections are difficult to observe.

Since coherent and incoherent emissions are two extreme cases of the phases  $\theta_j$  in Eq. (4) (perfectly uniform and random), a sharp distinction between the coherent and incoherent emissions is not always possible. Furthermore, the value  $\theta$  might change from  $\pi$  as we have seen for 319 layers sample, and unfortunately, there seems to be no clue for predicting the  $\theta$  value in our theoretical framework. The most proper method to calculate the reflectance is to derive a dynamical model controlling  $\theta_j$  of Eq. (4) from more a microscopic level,<sup>31,40</sup> and use it to calculate

$$R_N = \left| c_N^r + \sum_{j=1}^N e^{i\theta_j} Z_j(\mathcal{B}) \right|^2. \quad (10)$$

For the coherent photon emissions to be stabilized, there must be a mechanism for developing correlations between different layers. We speculate that motions of photoexcited electrons at the nearest-neighbor layers are mutually synchronized with each other through instantaneous Coulomb interaction. Because the photoexcited electrons in each graphene layer are described as the pseudospin flip,<sup>34,40</sup> the interaction can lead to a spatial order of pseudospins which may be involved in synchronization of the induced emission.

To conclude, we succeeded in explaining the measured visible contrasts of multilayer graphene samples on an SiO<sub>2</sub>/Si substrate by including coherent light emissions caused by some fraction ( $\mathcal{B}_{sti} = 0.0007$ ) of the absorbed photon energy. The coherent corrections are essential for assuring an agreement between theory and experiment, while the incoherent corrections could be neglected for the contrast. This research framework developed for  $N$ -layer graphene is applicable to other layered materials and will advance the use of layered materials in applications such as surface-emitting lasers.

## ACKNOWLEDGMENTS

K. S thanks Y. Sekine, H. Endo, and Y. Taniyasu for raising helpful questions on this subject. Part of this work was supported by “Nanotechnology Platform Japan” of the Ministry of Education, Culture, Sports, Science and Technology (MEXT), Grant Number

JPMXP09F21UT0045. The reflectance measurement was conducted in the Takeda Cleanroom with help of the Nanofabrication Platform Center of the School of Engineering, the University of Tokyo, Japan.

### Appendix A: Determination of $\varepsilon_r$ in Eq. (1)

We assume the bare permittivity of multilayer graphene (without corrections) is of the form of Eq. (1), where  $\varepsilon_r = 4$  in the main text. The choice is based on the following observations. First, there must not be a large discrepancy between  $\varepsilon_g$  and the experimentally determined optical constants.<sup>26,27</sup> The experimental  $n$  and  $k$  values, reported for chemical vapor deposited (CVD) graphene on SiO<sub>2</sub>/Si substrates in Ref. 27, are shown as circles in Fig. 5(a). Meanwhile, the lines are the optical constants plotted using Eq. (1) with refractive index  $n = \text{Re}[\sqrt{\varepsilon_g}]$  and absorption coefficient  $k = \text{Im}[\sqrt{\varepsilon_g}]$  for  $\varepsilon_r = 4$  and 1. A comparison between the measured and calculated values indicates that  $\varepsilon_r = 4$  is a reasonable value. Second,  $\varepsilon_g$  has to roughly reproduce the behavior of the reflectance of multilayer graphene. It takes a minimum at a certain wavelength primarily due to the destructive interference caused by SiO<sub>2</sub>. The position is red-shifted by increasing the layer number, as shown in Fig. 5(b). When  $\varepsilon_r = 1$ , a sizable artificial shift in the wavelength is needed to secure a reasonable agreement between theory and experiment. When  $\varepsilon_r = 4$ , a small difference between theory and experiment remains. However, the coherent corrections provide better agreement between not only the wavelengths giving minimum reflectivity but also the minimum reflectivity values and thus can account for the difference. Furthermore, it is the value that well reproduces the reflectivity of graphite in the infrared region.<sup>41</sup>

The experimental  $n$  and  $k$  values shown as circles in Fig. 5(a) are well fitted by the Drude–Lorentz oscillator model in Ref. 27. The corrections to the real part of the dielectric constant are mainly expressed as the Lorentz oscillator term, while in our transfer matrix formulation  $\varepsilon_r$  corresponds to the dielectric constant of the interlayer space. These descriptions are consistent with each other since the  $\pi$ -orbital spreads into the space outside of a graphene layer, and light propagating in the space is subjected to the spread of the wave function.<sup>25</sup>

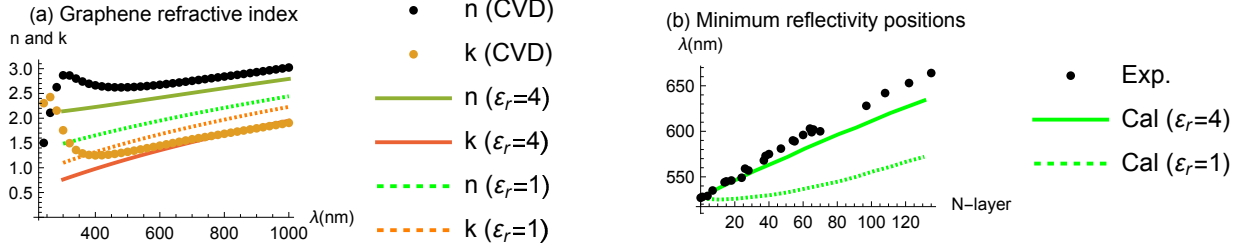


FIG. 5. (a) Dots are experimental  $n$  and  $k$  values, taken from Ref. 27, for CVD graphene on SiO<sub>2</sub>/Si substrates. (b) Dots are measured wavelengths that give the minimum reflectance. These comparisons between the measured and calculated results indicate that  $\epsilon_r = 4$  is a reasonable value.

### Appendix B: Measured reflectivities

We performed the reflectivity measurements for the same sample three times (run 1, run 2, and run 3). All measurements are consistent in the sense that the measured reflectivity of  $N$ -layer graphene on the substrate ( $R_N$ ) divided by that of the SiO<sub>2</sub>/Si substrate ( $R_0$ ), that is, the contrast ( $C_N = R_N/R_0$ ), are identical. Therefore, we compared  $C_N$  with calculations in the main text. However, while  $R_0$  of run 2 and run 3 were identical,  $R_0$  of run 1 was deviated from that of run 2 (run 3) as shown in Fig. 6. The same contrast also means that  $R_N$  of run 2 and run 3 are identical, while  $R_N$  of run 1 is deviated from that of run 2 (run 3) [Fig. 7]. The discrepancy between  $R_0$  of run 1 and that of run 2 (run 3) was presumably brought about by a change in the focal point along the depth direction when a reference substrate was replaced with the target sample. This could change the incident light intensity and lead to a discrepancy of  $R_N$  between run 1 and run 2 (run 3).

A problem arises when we determine the  $d_{\text{SiO}_2}$  value from  $R_0$ . Considering the fact that the wavelength giving the reflectivity minimum is the same for the three runs, we can determine  $d_{\text{SiO}_2} = 268$  nm by assuming that  $n_{\text{SiO}_2}$  is the standard value ( $\simeq 1.46$ ).<sup>30</sup> These parameters reasonably reproduce  $R_0$  of run 2 (run 3) [Fig. 6]. Meanwhile, 268 nm is inconsistent with another estimation using a reflectometer ( $274 \pm 1$  nm), which results in  $n_{\text{SiO}_2} \simeq 1.43$  to reproduce the wavelength giving the reflectivity minimum by destructive interference (same  $n_{\text{SiO}_2} d_{\text{SiO}_2}$ ). When we adopt  $n_{\text{SiO}_2} \simeq 1.43$  for  $d_{\text{SiO}_2} = 274$  nm, the corresponding  $R_0$  is the (blue) dashed curve, which reproduces  $R_0$  of run 1 around the reflectivity minimum (the

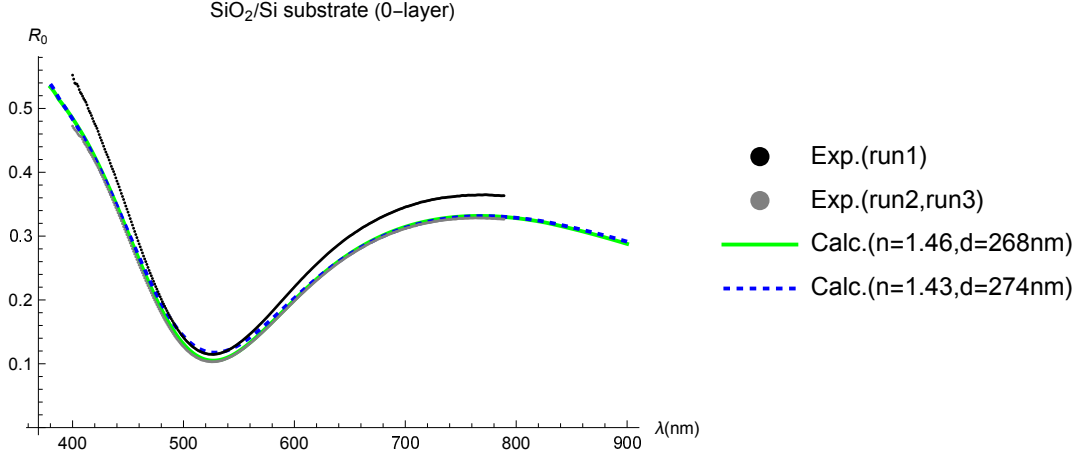


FIG. 6. Measured (black [run 1] and gray [run 2 (run 3)] dots) and calculated (green and blue dashed curves) spectral reflectivities of the same  $\text{SiO}_2/\text{Si}$  substrate. A white-light source was used, and the reflectivity was measured at room temperature. The horizontal axis is  $\lambda$  (nm), and the reliable range of our spectrometer is 450 to 800 nm.

two curves overlap from 460 to 560 nm) and approaches  $R_0$  of run 2 (run 3) away from the reflectivity minimum ( $\lambda < 460$  nm and  $\lambda > 560$  nm). Since  $n_{\text{SiO}_2} \simeq 1.43$  is an acceptable value, we need to mind the possibility that a true  $R_0$  is neither  $R_0$  of run 1 nor that of run 2 (run 3). Because we are assuming the refractive index of Si as the commonly used value, we keep the same standpoint for  $\text{SiO}_2$ . Finally we concluded  $d_{\text{SiO}_2} = 268$  nm.

In Fig. 7 we show the measured  $R_N$  and compare them with the calculated ones. Let us take the 122-layer sample as an example, in which  $R_{122}$  of run 1 is displaced by a constant factor from that of run 2 (run 3). This is consistent with the fact that  $R_N/R_0$  is universal because  $R_0$  is also displaced by a constant factor. The calculated  $R_N/R_0$  well reproduces the measured one, while the calculated  $R_N$  switches between the measured reflectivities of the different runs: for  $\lambda < 60$  nm, the red curve is on run 2; for  $\lambda > 700$  nm, it is close to run 1.

### Appendix C: Raman scattering as incoherent photons

We measured the  $G$ -band Raman peak intensity as a function of the thickness of multilayer graphene in order to inspect the interpretation of Raman scattering as the incoherent light emission.<sup>10</sup> As shown in Fig. 8, there is a reasonable similarity between the measured Raman

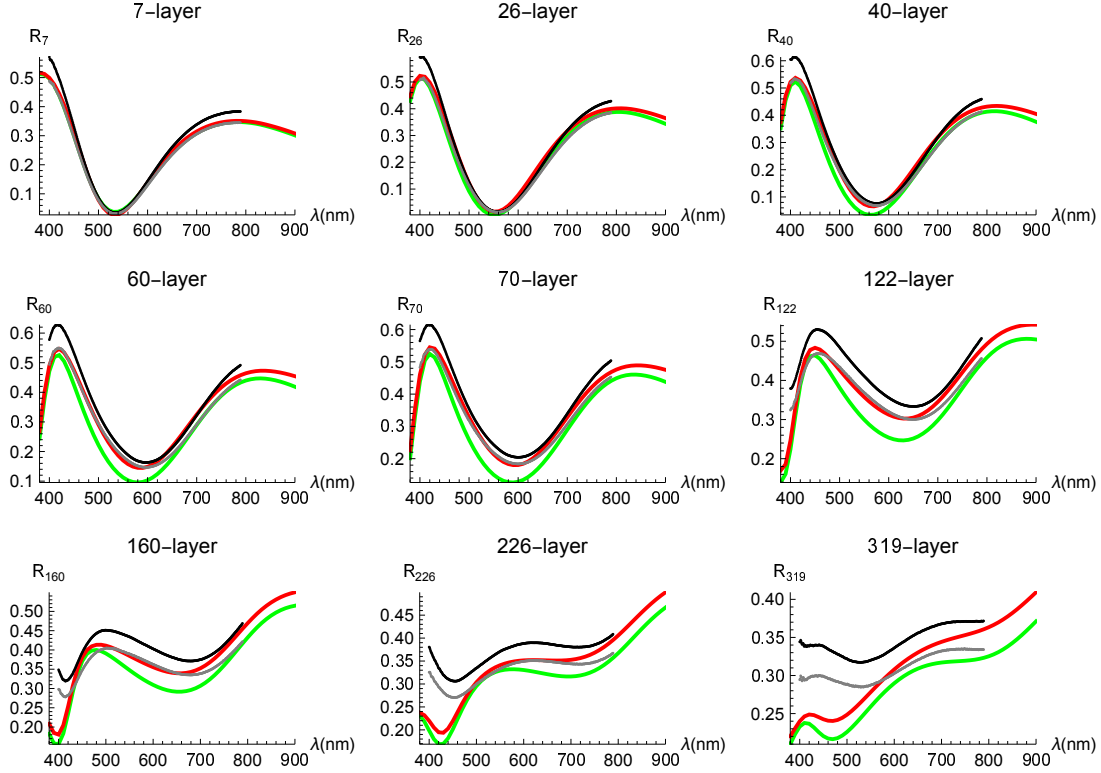


FIG. 7. Measured (black [run 1] and gray [run 2 (run 3)] dots) and calculated (green and red curves) spectral reflectivities of  $N$ -layer graphene on the same  $\text{SiO}_2/\text{Si}$  substrate. The green curves of Eq. (2) do not include corrections. The red curves include only coherent corrections.

intensity (dots) and calculated incoherent component (dashed curve). On the other hand, there is a discrepancy between them below 10 nm in thickness, where we notice a dip in the reflectance which is similar to the observation by No *et al.*<sup>39</sup> The assumption of random phase for  $\theta_j$  in Eq. (4) is a possible reason for the discrepancy, because random phases can undergo synchronization or entrainment.<sup>31</sup> An intermediate state of the phase  $\theta_j$  that is neither random nor perfectly coherent, may account for the behavior.

---

\* kenichi.sasaki.af@hco.ntt.co.jp

† Tomohiro.Matsui@anritsu.com

<sup>1</sup> K. S. Novoselov, A. K. Geim, S. V. Morozov, D. Jiang, M. I. Katsnelson, I. V. Grigorieva, S. V. Dubonos, and A. A. Firsov, *Nature* **438**, 197 (2005).

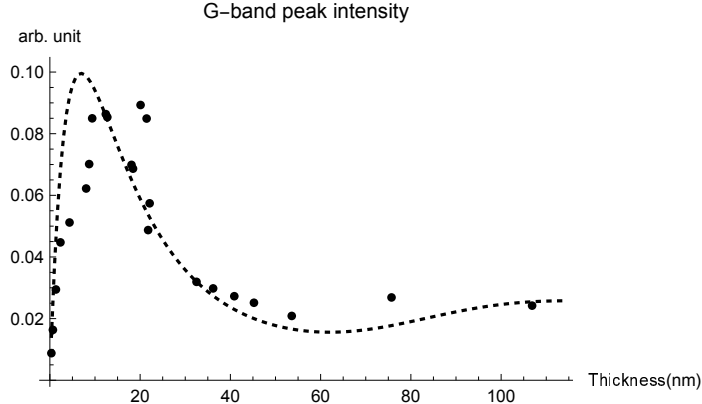


FIG. 8. Dots are the measured peak intensity of the Raman *G*-band using a light-source with wavelength 532 nm, and dashed curve is the incoherent correction. For thin multilayer graphene (below 10 nm thickness), we notice a dip in the reflectance which may indicate synchronization of Raman scattering.

- <sup>2</sup> Y. Zhang, Y.-W. Tan, H. L. Stormer, and P. Kim, *Nature* **438**, 201 (2005).
- <sup>3</sup> K. S. Novoselov, D. Jiang, F. Schedin, T. J. Booth, V. V. Khotkevich, S. V. Morozov, and A. K. Geim, *Proceedings of the National Academy of Sciences of the United States of America* **102**, 10451 (2005).
- <sup>4</sup> P. Blake, E. W. Hill, A. H. C. Neto, K. S. Novoselov, D. Jiang, R. Yang, T. J. Booth, and A. K. Geim, *Applied Physics Letters* **91**, 063124 (2007).
- <sup>5</sup> S. Roddaro, P. Pingue, V. Piazza, V. Pellegrini, and F. Beltram, *Nano Letters* **7**, 2707 (2007).
- <sup>6</sup> Z. H. Ni, H. M. Wang, J. Kasim, H. M. Fan, T. Yu, Y. H. Wu, Y. P. Feng, and Z. X. Shen, *Nano Letters* **7**, 2758 (2007).
- <sup>7</sup> C. Casiraghi, A. Hartschuh, E. Lidorikis, H. Qian, H. Harutyunyan, T. Gokus, K. S. Novoselov, and A. C. Ferrari, *Nano Letters* **7**, 2711 (2007).
- <sup>8</sup> B. G. Ghamsari, J. Tosado, M. Yamamoto, M. S. Fuhrer, and S. M. Anlage, *Scientific Reports* **6**, 1 (2016).
- <sup>9</sup> R. J. Nemanich, C. C. Tsai, and G. A. N. Connell, *Physical Review Letters* **44**, 273 (1980).
- <sup>10</sup> Y. Y. Wang, Z. H. Ni, Z. X. Shen, H. M. Wang, and Y. H. Wu, *Applied Physics Letters* **92**, 043121 (2008).
- <sup>11</sup> R. J. Stöhr, R. Kolesov, J. Pflaum, and J. Wrachtrup, *Physical Review B* **82**, 121408 (2010), arXiv:1006.5434.

- <sup>12</sup> C. H. Lui, K. F. Mak, J. Shan, and T. F. Heinz, *Physical Review Letters* **105**, 127404 (2010).
- <sup>13</sup> W. T. Liu, S. W. Wu, P. J. Schuck, M. Salmeron, Y. R. Shen, and F. Wang, *Physical Review B* **82**, 081408 (2010).
- <sup>14</sup> A. Riaz, F. Pyatkov, A. Alam, S. Dehm, A. Felten, V. S. Chakravadhanula, B. S. Flavel, C. Kübel, U. Lemmer, and R. Krupke, *Nanotechnology* **26**, 325202 (2015).
- <sup>15</sup> K. Sasaki and K. Hitachi, *Communications Physics* **3**, 90 (2020).
- <sup>16</sup> E. Hendry, P. J. Hale, J. Moger, A. K. Savchenko, and S. A. Mikhailov, *Physical Review Letters* **105**, 097401 (2010).
- <sup>17</sup> Z. Sun, T. Hasan, F. Torrisi, D. Popa, G. Privitera, F. Wang, F. Bonaccorso, D. M. Basko, and A. C. Ferrari, *ACS Nano* **4**, 803 (2010), arXiv:0909.0457.
- <sup>18</sup> S. A. Mikhailov, *Physica E: Low-dimensional Systems and Nanostructures* **44**, 924 (2012).
- <sup>19</sup> H. Yang, H. Guan, N. Biekert, G. Arefe, D. C. Chang, Y. Sun, P. C. Yeh, X. Liu, S. Y. Hong, I. D. Marion, M. Kralj, J. C. Hone, R. M. Osgood, and J. I. Dadap, *Physical Review Materials* **2**, 071002 (2018).
- <sup>20</sup> T. Ando, Y. Zheng, and H. Suzuura, *Journal of the Physical Society of Japan* **71**, 1318 (2002).
- <sup>21</sup> R. R. Nair, P. Blake, A. N. Grigorenko, K. S. Novoselov, T. J. Booth, T. Stauber, N. M. R. Peres, and A. K. Geim, *Science* **320**, 1308 (2008).
- <sup>22</sup> E. A. Taft and H. R. Philipp, *Physical Review* **138**, A197 (1965).
- <sup>23</sup> Y. H. Ichikawa and K. Kobayashi, *Carbon* **3**, 401 (1966).
- <sup>24</sup> M. S. Dresselhaus and G. Dresselhaus, *Physical Review B* **13**, 4635 (1976).
- <sup>25</sup> K.-i. Sasaki, *Journal of the Physical Society of Japan* **89**, 094706 (2020).
- <sup>26</sup> M. Bruna and S. Borini, *Applied Physics Letters* **94**, 031901 (2009).
- <sup>27</sup> M. A. El-Sayed, G. A. Ermolaev, K. V. Voronin, R. I. Romanov, G. I. Tselikov, D. I. Yakubovsky, N. V. Doroshina, A. B. Nemtsov, V. R. Solovey, A. A. Voronov, S. M. Novikov, A. A. Vyshnevyy, A. M. Markeev, A. V. Arsenin, and V. S. Volkov, *Nanomaterials* 2021, Vol. 11, Page 1230 **11**, 1230 (2021).
- <sup>28</sup> H. Anders, *Thin Films in Optics* (The Focal Press, 1965).
- <sup>29</sup> D. E. Aspnes and A. A. Studna, *Physical Review B* **27**, 985 (1983).
- <sup>30</sup> I. H. Malitson, *J. Opt. Soc. Am.* **55**, 1205 (1965).
- <sup>31</sup> Y. Kuramoto, *Springer Series in Synergetics*, **19** (1984), 10.1007/978-3-642-69689-3.
- <sup>32</sup> A. V. Durrant, *American Journal of Physics* **44**, 630 (1998).

- <sup>33</sup> M. Cray, M. Shih, and P. W. Milonni, *American Journal of Physics* **50**, 1016 (1998).
- <sup>34</sup> K.-i. Sasaki, K. Kato, Y. Tokura, K. Oguri, and T. Sogawa, *Physical Review B* **84**, 085458 (2011).
- <sup>35</sup> N. V. Velson, N. V. Velson, H. Zobeiri, X. Wang, and X. Wang, *Optics Express*, Vol. 28, Issue 23, pp. 35272-35283 **28**, 35272 (2020).
- <sup>36</sup> Strictly speaking, for the incoherent corrections,  $A_j^N$  should be calculated with  $\omega_e$ . We assume that  $A_j^N(\omega_e)$  is approximately the same as  $A_j^N(\omega)$ .
- <sup>37</sup> D. Yoon, H. Moon, H. Cheong, J. S. Choi, J. A. Choi, and B. H. Park, *Journal of the Korean Physical Society* **55**, 1299 (2009).
- <sup>38</sup> X. L. Li, X. F. Qiao, W. P. Han, Y. Lu, Q. H. Tan, X. L. Liu, and P. H. Tan, *Nanoscale* **7**, 8135 (2015).
- <sup>39</sup> Y. S. No, H. K. Choi, J. S. Kim, H. Kim, Y. J. Yu, C. G. Choi, and J. S. Choi, *Scientific Reports* **8**, 1 (2018).
- <sup>40</sup> R. H. Dicke, *Physical Review* **93**, 99 (1954).
- <sup>41</sup> A. B. Djurišić and E. H. Li, *Journal of Applied Physics* **85**, 7404 (1999).